Two-Dimensional Dielectric Profile Reconstruction Based on Spectral-Domain Moment Method and Nonlinear Optimization

Theofanis A. Maniatis, *Member, IEEE*, Konstantina S. Nikita, *Senior Member, IEEE*, and Nikolaos K. Uzunoglu, *Senior Member, IEEE*

***Abstract*—A novel method for two-dimensional (2-D) profile reconstruction of dielectric objects, based on nonlinear optimization, is presented in this paper. The unknown dielectric profile is expressed in terms of Gaussian basis functions. The scattering integral equation (SIE) is discretized using a spectral-domain moment technique, where the unknown internal field is described as a superposition of a limited number of plane waves, resulting in a significant reduction of the associated computational cost. The inverse-scattering problem is solved by minimizing a cost function consisting of two terms: the first term represents the error between measured and predicted values of the scattered field, while the second term corresponds to the error in satisfying the SIE for the field in the interior of the scatterer. Accurate and efficient dielectric profile reconstructions of 2-D lossy scatterers of circular and square cross sections using synthetic scattered field data are presented, while the effect of various discretization parameters on the convergence of the method is studied in detail.**

***Index Terms*—Biomedical imaging, electromagnetic scattering inverse problems, optimization methods.**

I. Introduction

MICROWAVE imaging of biological objects is highly desirable since it provides quantitative information about dielectric properties of tissues, which cannot be estimated *in vivo* by any of the currently available medical-imaging modalities, and may potentially relate to the physiological state of the tissue. A key step for the implementation of quantitative microwave imaging is the efficient solution of the associated inverse-scattering problem.

Early methods in inverse scattering were based on the linearization of the problem using the first-order Born or Rytov approximation [1], [2]. Despite their mathematical simplicity, these methods are useful only for small and/or weakly scattering objects [3]. In order to overcome the stringent limitations imposed by the first-order linear methods, nonlinear methods have also been suggested [4], [5].

Spatial-domain techniques have been presented based on the discretization of the exact scattering integral equations (SIEs) by means of the method of moments (MoM). One of the earliest approaches has been based on the solution of the equation for the field inside the scatterer and subsequent substitution to the equation for the measured scattered field, seeking a direct solution of the inverse-scattering problem [6]. Unfortunately, this method suffered from the serious ill-posedness of the inverse problem. To alleviate this problem, pseudoinversion techniques in conjunction with redundant scattered field data have been suggested [7], [8].

Alternative approaches have been based on the reformulation of the inverse problem as a nonlinear optimization one and its solution using either Newton-type iterative procedures [9]–[16] or the modified gradient method [17], [18]. Lately, a contrast source inversion method has been suggested, improving the overall performance of the modified gradient method [19], [20]. In order to overcome the numerical complexity associated with object sizes found in medical imaging, a method has been presented that restricts the investigation domain in a subregion of the human body [21].

Other interesting approaches have introduced the use of the finite-element method or its hybrid coupling with the boundary-element method, for the direct scattering problem, while the inversion is based on conjugate-gradient [22] or Newton's [23] iterative schemes, respectively.

Although most of the above nonlinear methods have no theoretical restriction regarding the size or the refractive index of the scattering object, they usually lead to an increased number of unknowns for any problem of practical importance.

In order to demonstrate the practical implementation of various inverse-scattering methods, several experimental prototypes for microwave imaging of biological tissues have been developed, operating at various frequencies in the range of 300 MHz–2.45 GHz [24]–[29]. The early prototype [26] has been based on linear inversion algorithms (i.e., Born approximation) providing rather qualitative reconstructed images. However, more recent approaches adopt quantitative—usually iterative—reconstruction algorithms with the cost of heavy computational requirements [25], [27]–[29].

In this paper, a novel method based on a spectral-domain MoM technique is presented, suitable for microwave imaging of biological objects. The interaction of the incident field with the scattering object is described in terms of the Lippmann—Schwinger SIE. The unknown total wave field inside the scattering object is expressed as a superposition of a relatively small number of global domain basis functions (i.e., plane waves), while the unknown object function is expanded in a set of spatially shifted Gaussian basis functions. The

Manuscript received November 12, 1999; revised May 3, 2000.

The authors are with Department of Electrical and Computer Engineering, National Technical University of Athens, 15780 Athens, Greece (e-mail: knikita@cc.ece.ntua.gr).

Publisher Item Identifier S 0018-9480(00)09534-X.

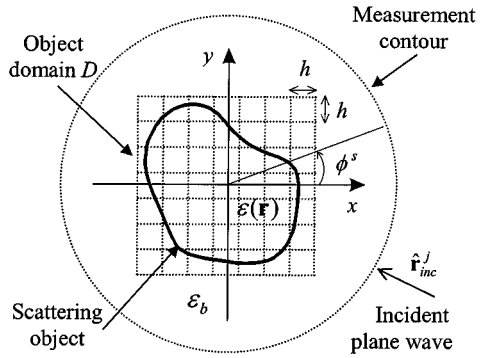

Fig. 1. Problem geometry with the object domain and Cartesian grid.

inverse-scattering problem is formulated as a nonlinear optimization problem, which is solved by employing the modified gradient method [17]. The main advantage of the proposed formulation lies in the use of global-domain basis functions, leading to a significant decrease of the number of unknowns and, consequently, to a substantially lower computational cost.

This paper is organized in the following manner. The formulation and solution of the direct and inverse-scattering problems are presented in Section II. In Section III, the necessary checks for the validation of the proposed method are described, followed by dielectric-permittivity reconstructions of lossy dielectric cylinders, based on the use of synthetic scattered field data. In Section IV, important features of the method and directions for further development are discussed.

II. Mathematical Formulation and Analysis

A. Formulation of the Direct Problem

In this paper, we limit ourselves to two-dimensional (2-D) problems. Let us consider a plane monochromatic wave[1] $\psi_0(\mathbf{r}) = \exp(ik_b\hat{\mathbf{r}}^j_{\mathbf{inc}} \cdot \mathbf{r})$ propagating in the direction $\hat{\mathbf{r}}^j_{\mathbf{inc}}$ inside an isotropic homogeneous medium, with wavenumber $k_b = \omega\sqrt{\varepsilon_b\mu_b}$, where ω is the angular frequency, ε_b and $\mu_b = \mu_0$ are the medium's dielectric permittivity and magnetic permeability, respectively, with μ_0 being the free-space magnetic permeability. The wave impinges on a scattering object characterized by the complex dielectric permittivity $\varepsilon(\mathbf{r})$, as shown in Fig. 1. The magnetic properties of the object are defined as $\mu(\mathbf{r}) = \mu_0$, which is appropriate for biological media.

The wave propagation is governed by the scalar Helmholtz equation provided that the incident wave is pure TM and no depolarization effects take place within the scattering object. The scattered field is measured in the far region at a number of $s = 1, \ldots, S$ points located at directions $\hat{\mathbf{r}}^s_{sc}$ (corresponding to the observation angles ϕ^s) along a circular contour that fully encloses the scattering object (Fig. 1). The measurement procedure can be repeated for a number of different incident field directions $\hat{\mathbf{r}}^j_{\mathbf{inc}}$, $j = 1, \ldots, J$. A Cartesian grid consisting of N_g cells ($\Delta x = \Delta y = h$) is defined within the object domain D, which totally covers the scattering object (Fig. 1).

[1]A time dependence $e^{-i\omega t}$ is assumed and omitted throughout.

The total field at any spatial location is given by the Lippmann–Schwinger SIE

$$\psi(\mathbf{r}) = \psi_0(\mathbf{r}) + k_b^2 \int_D d\mathbf{r}' o(\mathbf{r}')\psi(\mathbf{r}')g(\mathbf{r}|\mathbf{r}') \tag{1}$$

where $g(\mathbf{r}|\mathbf{r}')$ is the 2-D Green's function given by

$$g(\mathbf{r}|\mathbf{r}') = \frac{i}{4} H_0(k_b|\mathbf{r} - \mathbf{r}'|)$$

with H_0 being the zeroth-order Hankel function of the first kind. The object function $o(\mathbf{r})$ is defined as

$$o(\mathbf{r}) = n_r^2(\mathbf{r}) - 1$$

where $n_r^2(\mathbf{r}) = \varepsilon(\mathbf{r})/\varepsilon_b$ is the complex refractive index of the scatterer. The object function is expanded into N_g spatially shifted Gaussian basis functions

$$o(\mathbf{r}) \cong \sum_{n=1}^{N_g} \alpha_n e^{-((\mathbf{r}-\mathbf{r}_n)^2/\tau^2)} \tag{2}$$

where α_n are coefficients, which are known for the direct scattering problem and should be determined for the inverse problem. The centers of the Gaussian basis functions coincide with the centers of the grid cells $\mathbf{r}_n$. The width of the Gaussian functions is denoted by τ and considered to be equal to the object-domain grid spacing $\tau = h$.

The scattering amplitude at an observation direction $\hat{\mathbf{r}}^s_{sc}$ expresses the asymptotic behavior of the scattered field in the far region, and is defined as [30]

$$f_a(\hat{\mathbf{r}}^s_{sc}) = e^{i(\pi/4)}\sqrt{\frac{k_b^3}{8\pi}} \int_D d\mathbf{r}' e^{-ik_b\hat{\mathbf{r}}^s_{sc}\cdot\mathbf{r}'} o(\mathbf{r}')\psi(\mathbf{r}'). \tag{3}$$

The total field in the interior of the scattering object can be expressed as a superposition of plane waves

$$\begin{aligned}\psi(\mathbf{r}) &= \frac{1}{(2\pi)^2} \int_{-\infty}^{\infty} dp_x \int_{-\infty}^{\infty} dp_y e^{i\mathbf{pr}} C(\mathbf{p}) \\ &= \frac{1}{(2\pi)^2} \int_{\Omega} d\mathbf{p} e^{i\mathbf{pr}} C(\mathbf{p})\end{aligned} \tag{4}$$

where $C(\mathbf{p})$ is the Fourier transform of the field inside the scatterer. By substituting (4) into (1), multiplying both sides by the object function, and taking the Fourier transform, we obtain

$$\int_{\Omega} d\mathbf{p} C^j(\mathbf{p})\left[O(\mathbf{q}-\mathbf{p}) - \lambda^{-2} I(\mathbf{q}, \mathbf{p})\right] = (2\pi)^2 O(\mathbf{q}-\mathbf{k}^j_{\mathbf{inc}}), \quad j = 1, \ldots, J \tag{5}$$

where $\lambda = 2\pi/k_b$ is the wavelength in the host medium, $O(\mathbf{k})$ denotes the Fourier transform of the object function, and the superscript j denotes the dependence of the total wave field on the incident plane wave, propagating in the direction of $\mathbf{k}^j_{\mathbf{inc}} = k_b\hat{\mathbf{r}}^j_{\mathbf{inc}}$. The term $I(\mathbf{q}, \mathbf{p})$ is given by the integral

$$I(\mathbf{q}, \mathbf{p}) = \int_{\Omega} d\mathbf{k} \frac{O(\mathbf{q}-\mathbf{k})O(\mathbf{k}-\mathbf{p})}{k^2 - k_b^2}. \tag{6}$$

Similarly, by substituting (4) into (3), the scattering amplitude is expressed as follows:

$$f_a^j(\mathbf{k}_{sc}^s) = e^{i(\pi/4)}\frac{\lambda^{-3/2}}{4\pi}\int_\Omega d\mathbf{p}C^j(\mathbf{p})O(\mathbf{k}_{sc}^s - \mathbf{p}) \quad (7)$$

where $\mathbf{k}_{sc}^s = k_b\hat{\mathbf{r}}_{sc}^s$. A key procedure in the proposed formulation is the discretization of the spectral-domain integrals (5) and (7), using a finite number of wave vectors $\{\mathbf{p}_l\}$. This is equivalent to expanding the total internal field in plane waves [see (4)] with wave vectors $\{\mathbf{p}_l\}$. Discretization of (5) and (7) [see Appendix], leads to the following equations written in matrix–vector notation:

$$\overline{\mathbf{U}}\mathbf{W}^j = \mathbf{O}^j, \quad (8)$$

$$f_{a,\,s}^j = e^{i(\pi/4)}\frac{\lambda^{-3/2}}{4\pi}(\mathbf{O}^s)^T\mathbf{W}^j, \qquad j = 1, \ldots, J; \quad s = 1, \ldots, S. \quad (9)$$

where the vectors $\mathbf{O}^j$ and $\mathbf{O}^s$ are related with the object function, while the vector $\mathbf{W}^j$ is related with the expansion of the internal field into plane waves. The elements of matrices and vectors appearing in (8) and (9) are given in detail in the Appendix.

The direct scattering problem can be solved using (8) and (9). In fact, if the dielectric profile of the scattering object is known, then (2) can be used to determine the Gaussian basis functions expansion coefficients (α_n) of the object function. Solution of the system of equations (8) with respect to the vector $\mathbf{W}^j$ for a given incident field direction $\hat{\mathbf{r}}_{\mathrm{inc}}^j$ and substitution into (9) provides the scattering amplitude.

B. Formulation and Solution of the Inverse Problem

For the solution of the inverse-scattering problem, we define the residual $\mathbf{P}^j$ that represents the error in satisfying the system of equations (8)

$$\mathbf{P}^j = \overline{\mathbf{U}}\mathbf{W}^j - \mathbf{O}^j, \qquad j = 1, \ldots, J. \quad (10)$$

In addition, a second residual term $\mathbf{R}^j$ is defined, representing the difference between the measured values of the scattering amplitude $\mathbf{f}_{\mathrm{meas}}^j$ and the theoretic prediction according to (9) for a number of S observation directions

$$\mathbf{R}^j = \mathbf{f}_{\mathrm{meas}}^j - e^{i(\pi/4)}\frac{\lambda^{-3/2}}{4\pi}\overline{\mathbf{O}}^{\mathrm{scat}}\mathbf{W}^j, \qquad j = 1, \ldots, J \quad (11)$$

where

$$\mathbf{f}_{\mathrm{meas}}^j = \left[f_{\mathrm{meas},\,1}^j, f_{\mathrm{meas},\,2}^j, \ldots, f_{\mathrm{meas},\,S}^j\right]^T$$

and the matrix $\overline{\mathbf{O}}^{\mathrm{scat}}$ is defined as

$$\overline{\mathbf{O}}^{\mathrm{scat}} = \left[\mathbf{O}^1, \mathbf{O}^2, \ldots, \mathbf{O}^S\right]^T.$$

A cost function Q is formed in terms of the residuals $\mathbf{P}^j$ and $\mathbf{R}^j$

$$Q\left(\boldsymbol{\alpha}, \mathbf{W}^1, \ldots, \mathbf{W}^J\right) = \sum_{j=1}^J \|\mathbf{P}^j\|_2^2 + \sum_{j=1}^J \|\mathbf{R}^j\|_2^2 \quad (12)$$

where $\|\cdot\|_2$ denotes the two-norm and the vector $\boldsymbol{\alpha}$ is defined as

$$\boldsymbol{\alpha} = \left[\alpha_1, \alpha_2, \ldots, \alpha_{N_g}\right]^T.$$

The inverse-scattering problem is formulated as the problem of minimizing the cost function Q with respect to the Gaussian basis-function expansion coefficients ($\boldsymbol{\alpha}$) of the object function and the expansion coefficients of the field inside the scatterer ($\mathbf{W}^j$). This nonlinear optimization problem is solved iteratively using the modified gradient method proposed by Kleinmann and Van den Berg [17], which does not require explicit solution of the direct scattering problem at each step of the minimization procedure.

III. Numerical Results

A. Direct Problem

The formulation presented thus far can be used for the solution of the direct scattering problem. The integral terms $I(\mathbf{q}, \mathbf{p})$ [see (6)] depend on the pair of wave vectors ($\mathbf{q}$, $\mathbf{p}$) and the set of Gaussian basis functions used for the discretization of the object function $o(\mathbf{r})$. The calculation of these 2-D Fourier integrals is performed analytically with respect to the angular variable, and numerically with respect to the radial. Furthermore, their calculation can be performed off-line and stored for subsequent usage, while significant computational savings can be achieved by exploiting some symmetry properties of the integrals $I(\mathbf{q}, \mathbf{p})$, as noted in the Appendix.

One of the main advantages of the proposed spectral-domain method is the ability to express the total internal wave field in terms of a relatively small number of plane waves, whereas spatial-domain methods require fine discretization of the internal wave field. Appropriate selection of the wave vectors used in discretizing (5) and (7) [see Appendix] can improve the performance of the method. In fact, the proposed method is expected to perform well if the magnitudes of the expansion wave vectors $\{\mathbf{p}_l\}$ [see (A1) and (A4)] are close to the propagation wavenumber within the scattering object.

In order to check the accuracy and convergence of the developed method, several checks have been performed. Let us consider a simple 2-D scattering object. It consists of a two-layer infinite-length cylinder whose refractive index is given by

$$n_r(\mathbf{r}) = \begin{cases} 0.81 + i\cdot 0.15, & \text{for } 0 \le r \le 0.8\lambda \\ 0.26 + i\cdot 0.03, & \text{for } 0.8\lambda < r \le \lambda \\ 1, & \text{for } r > \lambda. \end{cases}$$

Although not in scale, this scatterer represents a biological model, consisting of an outer bone layer and an inner brain core, which is immersed into deionized water. The complex relative permittivities of the tissue media, which are compiled from the relevant literature [31], [32], as well as the dielectric constant of the background medium, used in the calculations, are $\varepsilon_{\mathrm{bone}} = 5.1 + i\cdot 1.1$, $\varepsilon_{\mathrm{brain}} = 49 + i\cdot 18.5$, $\varepsilon_{\mathrm{water}} = 77$, at $f = 2\pi/\omega = 2.45$ GHz. We assume that the scatterer is illuminated by a plane wave propagating in the direction of $\hat{x}$ (see Fig. 1).

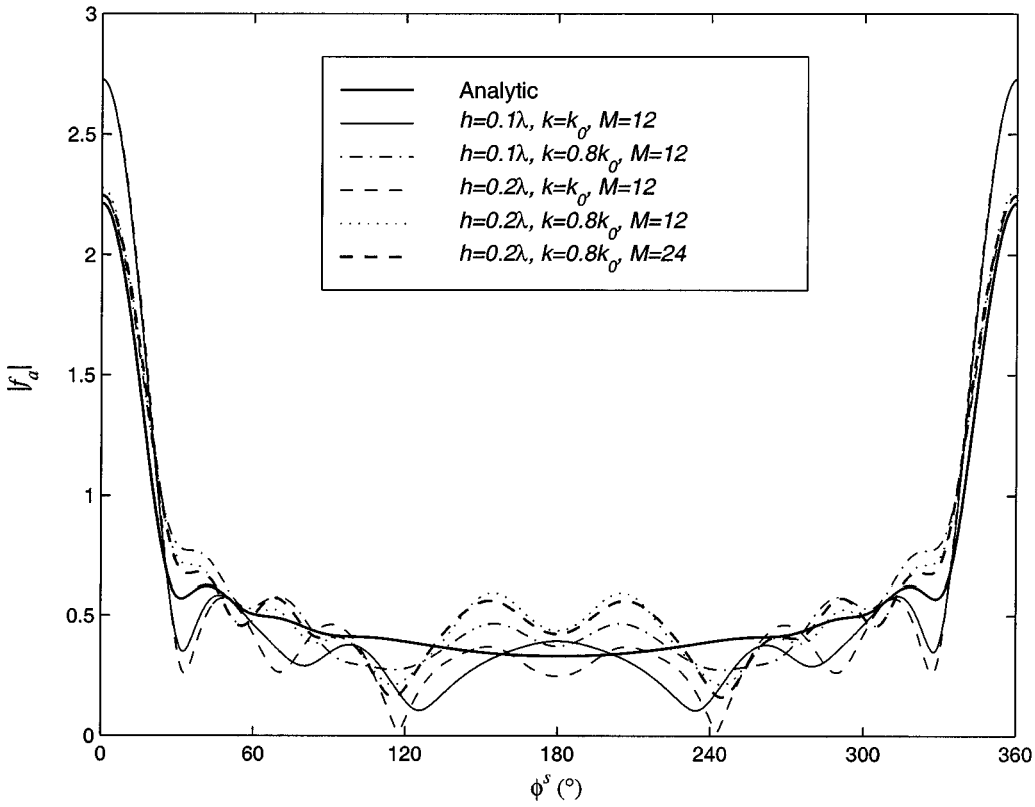

Fig. 2. Magnitude of the scattering amplitude as a function of the observation angle. The angle of incidence is 0°.

The effects of the spatial- and spectral-domain discretization are assessed using five different combinations of the discretization parameters. To this end, the scattering amplitude calculated by applying the proposed method is compared with that obtained analytically, using separation of variables and eigenfunction expansion. With respect to the spatial sampling of the object function, two distinct cases for the grid spacing are considered, namely, a fine grid ($h = 0.1\lambda$) and a coarse grid ($h = 0.2\lambda$), resulting in a total number of $N_g = 21 \times 21$ and $N_g = 11 \times 11$ Gaussian basis functions, respectively [see (2)]. Regarding the discretization of the spectral-domain integral equations, three sets of 2-D wave vectors $\{\mathbf{p}_l\}$ with uniform angular distribution from 0π to 2π [see Appendix, (A1) and (A4)] are used. The first two sets consist of $M = 12$ wave vectors each, with constant magnitude k_b and $0.8k_b$, respectively, while the third set consists of $M = 24$ wave vectors, with constant magnitude $0.8k_b$.

The magnitude of the scattering amplitude, as computed for five different combinations of spatial and spectral discretization parameters along the exact analytic solution, are plotted in Fig. 2 as a function of the observation angle. The most significant improvement on the accuracy of the calculated scattering amplitude is mainly due to the proper selection of the wave-vector set $\{\mathbf{p}_l\}$. Since the main portion of the scattering object is characterized by a refractive index of $n_r = 0.81 + i \cdot 0.15$, the wave-vector sets with magnitude of $0.8k_b$ are better suited for the description of the internal field. On the other hand, the spatial-domain grid spacing has a less significant effect on the accuracy of the calculated scattering amplitude, although the fine-grid case ($h = 0.1\lambda$) produces marginally better results compared with the coarse-grid case ($h = 0.2\lambda$). Furthermore, the use of 24 wave vectors slightly improves the accuracy of the calculated scattering amplitude, as compared with the use of 12 wave vectors.

B. Inverse Problem

The efficiency of the proposed inverse-scattering method for tomographic imaging of biological objects is demonstrated with the refractive index reconstruction of two different scattering objects. It is pointed out that in order to avoid any trivial inversion of the 2-D scattering problem, synthetic scattered field data should be obtained by a direct solver having no relation to the inverse method itself. Otherwise, a common mistake is committed, usually referred to as *inverse crime* [33].

As a first testing case, we consider the scattering object used in the previous paragraph. In terms of spatial-domain discretization, both fine and coarse-grid cases are studied, while in terms of spectral-domain discretization, a set of $M = 12$ wave vectors $\{\mathbf{p}_l\}$ with constant magnitude k_b and uniform angular distribution from 0π to 2π is considered.

The scattering object is illuminated by $J = 12$ plane waves and, for each illumination, a total of $S = 48$ scattering amplitude data, uniformly distributed along the measurement circle, are used. Synthetic scattering amplitude data have been calculated using the analytic solution.

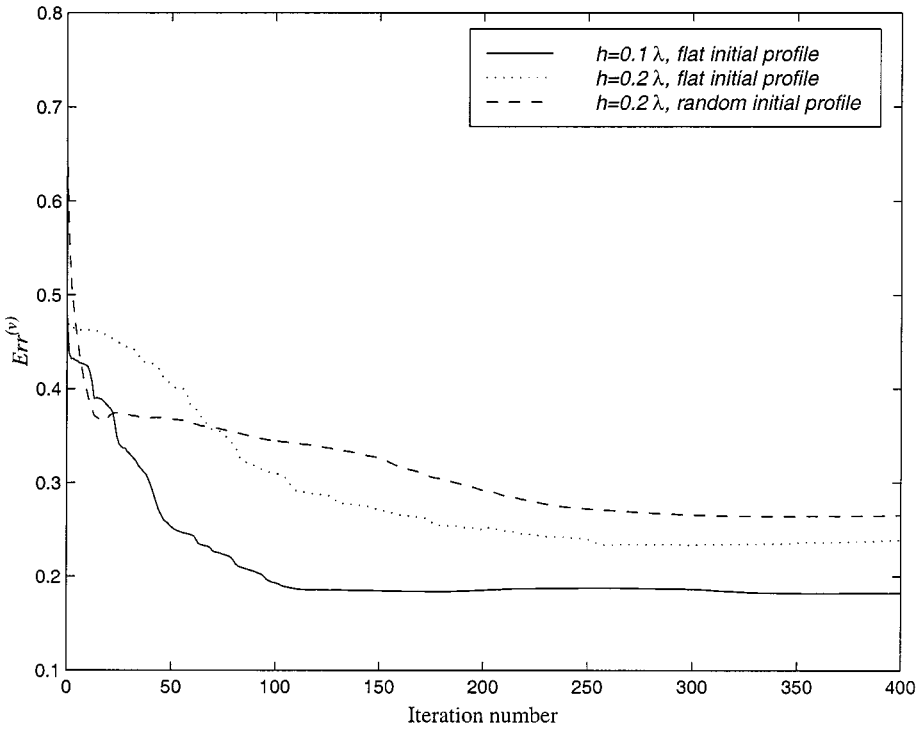

Fig. 3. Mean square reconstruction error as a function of iteration number. Solid line: fine-grid case with a flat initial profile. Dotted line: coarse-grid case with a flat initial profile. Dashed line: coarse-grid case with the random initial profile.

We define the mean square reconstruction error for the refractive index at the νth step of the iterative minimization procedure

$$\mathrm{Err}^{(\nu)} = \frac{\left\| n_r(\mathbf{r}) - n_r^{(\nu)}(\mathbf{r}) \right\|_2}{\left\| n_r(\mathbf{r}) \right\|_2} \tag{13}$$

as a figure-of-merit for the reconstructed profile. In (13), $n_r(\mathbf{r})$ represents the exact refractive index, while $n_r^{(\nu)}(\mathbf{r})$ represents the reconstructed one at the νth step.

In order to check the stability of the proposed inverse-scattering method, two different initial guesses for the scattering object's refractive index distribution have been considered. The first one consists of a flat square profile given by

$$n_r(\mathbf{r}) = \begin{cases} 1.01 + i \cdot 0.015, & \text{for } |x| \le 0.8\lambda \wedge |y| \le 0.8\lambda \\ 1, & \text{elsewhere.} \end{cases}$$

The second initial profile is totally random, following a normal distribution with mean value $\overline{n_r}(\mathbf{r}) = 0.9 + i \cdot 0.1$ and standard deviation of 0.2 for the real part and 0.1 for the imaginary part of the refractive index. A total of 400 iterations of the reconstruction procedure have been performed. In Fig. 3, the mean square reconstruction error is plotted as a function of the iteration number for the flat initial profile (fine and coarse-grid case) and the random initial profile (coarse-grid case). A rapid decrease of the reconstruction error after the first few iterations is observed for both grid cases, followed by a decrease at a relatively slower rate at subsequent iterations. However, the mean square reconstruction error for the fine grid is constantly lower than that for the coarse grid. Regarding the reconstruction starting from the random initial profile, a more rapid decrease of the mean square reconstruction error is observed at the first few iterations, while the final mean square reconstruction error is higher as compared with that obtained from the flat initial profile.

The exact and reconstructed profiles are shown in Fig. 4. Although the coarse-grid reconstruction [see Fig. 4(b) and (c)] retains the intelligibility of the object's profile, the use of the fine grid yields better reconstruction results [see Fig. 4(d)] in fewer iterations. Furthermore, the imaginary part of the bone's refractive index is poorly discriminated in both grid cases. This should be attributed to the low contrast of the imaginary part of the bone's refractive index compared with that of the background medium (water). For both grid cases, Gibbs-type phenomena are observed near the edges of the scatterer, which are more pronounced in the fine-grid case. This is due to the difficulty in describing abrupt changes in the dielectric profile with Gaussian basis functions. Finally, choosing a totally random initial profile yields similar reconstruction results [see Fig. 4(b)]. Therefore, we may conclude that the proposed method is stable with respect to the initial choice of the refractive index distribution. It should be noted that the random initial profile constitutes a worst-case scenario since one should always be able to find a better initial estimate using a linear inverse-scattering method (Born or Rytov). Improved reconstructions may be obtained by using a set of wave vectors $\{\mathbf{p}_l\}$ with magnitude $0.8k_b$, which has been shown to produce more accurate results for the direct problem.

Next, a lossy dielectric cylinder of a more complicated structure has been considered, having square cross section and con-

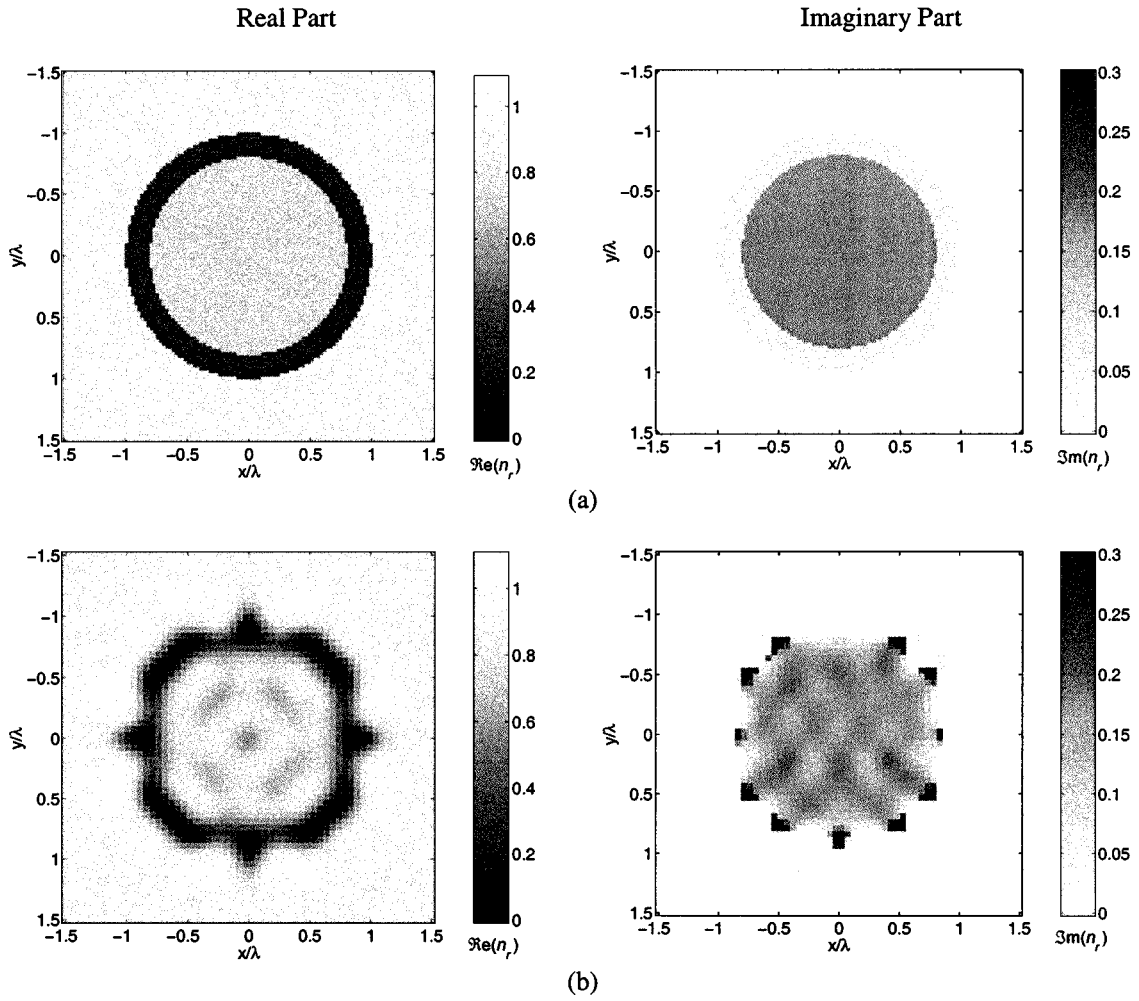

Fig. 4. Exact and reconstructed dielectric profiles. Real part of the refractive index is shown in the left-hand-side column and the imaginary part in the right-hand-side column. (a) Exact profile. (b) Reconstructed profile after 400 iterations (coarse grid) using a random initial profile.

sisting of eight subsections, as shown in Fig. 5. The distribution of the scatterer's refractive index is given by

$$n_r(\mathbf{r}) = \begin{cases} 1.4 + i \cdot 0.1, & \mathbf{r} \in D_1 \\ 1.5 + i \cdot 0.1, & \mathbf{r} \in D_2 \\ 1.3 + i \cdot 0.1, & \mathbf{r} \in D_3 \\ 1.2 + i \cdot 0.1, & \mathbf{r} \in D_4 \\ 1.4 + i \cdot 0.2, & \mathbf{r} \in D_5 \\ 1.5 + i \cdot 0.2, & \mathbf{r} \in D_6 \\ 1.3 + i \cdot 0.2, & \mathbf{r} \in D_7 \\ 1.2 + i \cdot 0.2, & \mathbf{r} \in D_8 \\ 1, & \text{elsewhere.} \end{cases}$$

The scattering object is illuminated by $J = 12$ plane waves and for each illumination a total of $S = 48$ scattering amplitude data, uniformly distributed along the measurement circle, are used. Synthetic scattering amplitude data have been generated using the MoM with pulse basis functions and point matching [34]. In this example, a coarse grid of $N_g = 21 \times 21$ Gaussian basis functions has been used ($h = 0.2\lambda$), covering the domain $\{|x| \leq 2\lambda \wedge |y| \leq 2\lambda\}$. Furthermore, a set of $M = 12$ wave vectors $\{\mathbf{p}_l\}$ with constant magnitude k_b and uniform angular distribution from 0π to 2π has been used for the spectral-domain discretization. The initial guess for the refractive index profile is

$$n_r(\mathbf{r}) = \begin{cases} 1.01 + i \cdot 0.015, & \text{for } |x| \leq 1.8\lambda \wedge |y| \leq 1.8\lambda \\ 1, & \text{elsewhere.} \end{cases}$$

A total of 400 iterations of the reconstruction procedure have been carried out. The exact and reconstructed profiles of the real and imaginary parts of the refractive index are shown in Fig. 6. In a qualitative sense, the algorithm seems to be able to discriminate the different subsections, performing slightly better for the real part of the complex refractive index than for the imaginary part.

Concerning the computational resources used, the developed algorithm was executed on a Pentium II 350 –MHz personal computer, and the average reconstruction time per iteration was 5 s for the circular cross-sectional object and coarse-grid case.

IV. Discussion

The main advantage of the proposed inverse-scattering method is the significant reduction of the total number of unknowns, which is related to the limited number of global-domain basis functions required for the description of the internal

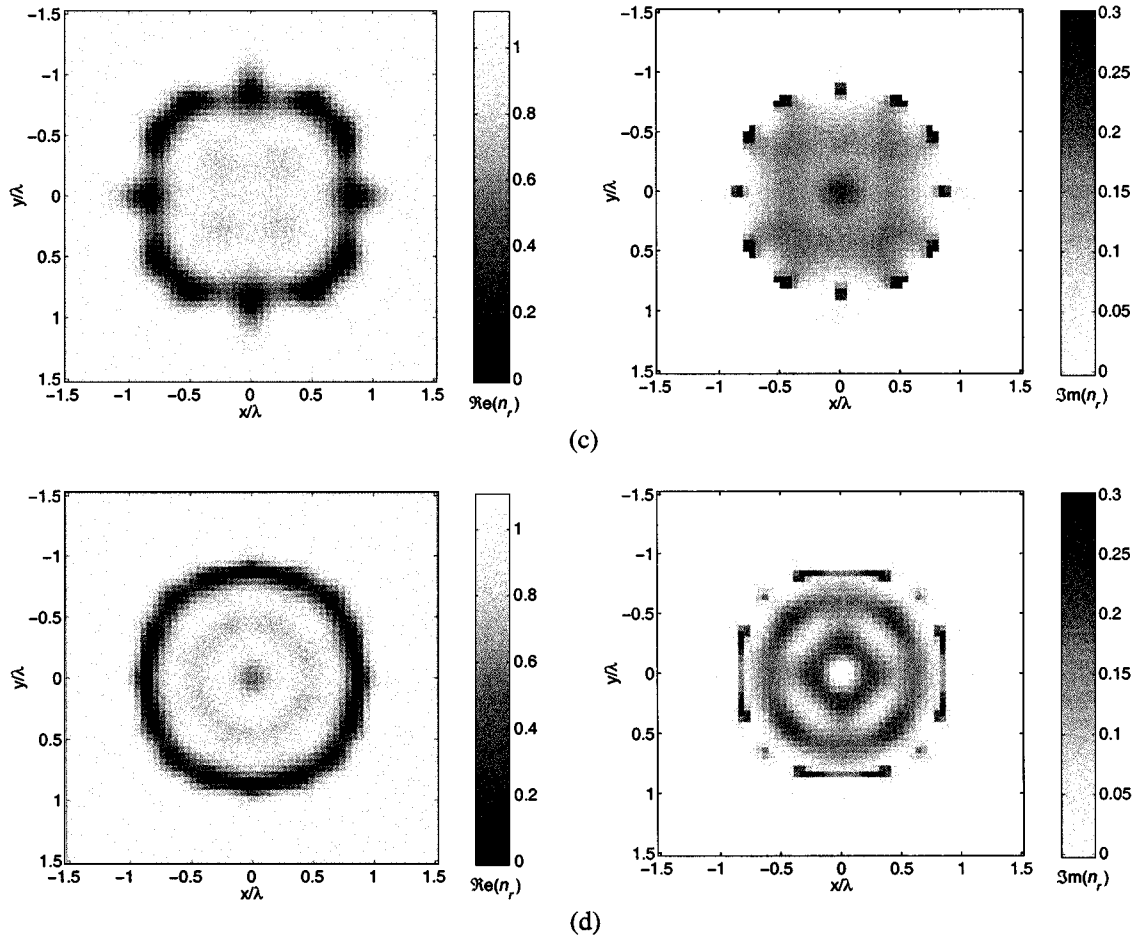

Fig. 4. *(Continued.)* Exact and reconstructed dielectric profiles. Real part of the refractive index is shown in the left-hand-side column and the imaginary part in the right-hand-side column. (c) Reconstructed profile after 400 iterations (coarse grid) using a flat initial profile. (d) Reconstructed profile after 200 iterations (fine grid) using a flat initial profile.

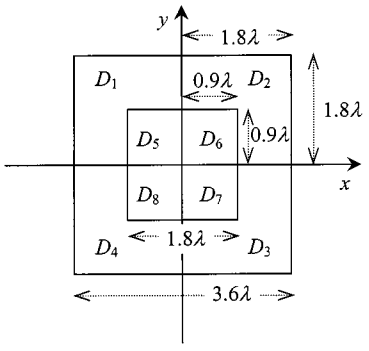

Fig. 5. Cross section of infinite length dielectric scatterer.

field. In optimization-type inverse-scattering techniques, based on the MoM in the spatial domain, the discretization required for the description of the object function leads to a number of N variables per λ^2, while an equal number of N variables per λ^2 per incident wave field is required for the description of the internal field, where $9 \leq N \leq 100$ [13], [17], [18], [20]. In contrast, the proposed formulation requires N variables per λ^2 for the description of the object function and a small number of variables (typically 12 per incident wave field) for the description of the internal field.

From the simulation results presented in Section III, it is evident that fine discretization of the object function yields better reconstruction results. However, it should be noted that even with coarse spatial-domain discretization ($h = 0.2\lambda$), fairly good images are acquired. Moreover, fine spatial discretization may not provide significant improvement of the reconstructed image quality, especially when experimental data are used, as is shown in [13] for a human forearm. In terms of the spectral-domain discretization, a uniform distribution of wave vectors in the angular direction seems to be adequate. Furthermore, if the magnitude of these wave vectors is selected to be close to the average propagation wavenumber within the scatterer, a better description of the internal field can be obtained. Although this information is not available in advance, a reasonable estimate can be deduced based on the general type of tissue being imaged.

The presented reconstruction algorithm can be further improved by introducing constraints for the object's refractive index (such as positivity constraints) [18]. Furthermore, *a priori* information available for biological tissues dielectric properties can also be included in the method. In fact, a good initial guess about the dielectric profile obtained by a linear inverse-scattering method (such as Born or Rytov [2]) may have beneficial effects to the convergence of the proposed method [13].

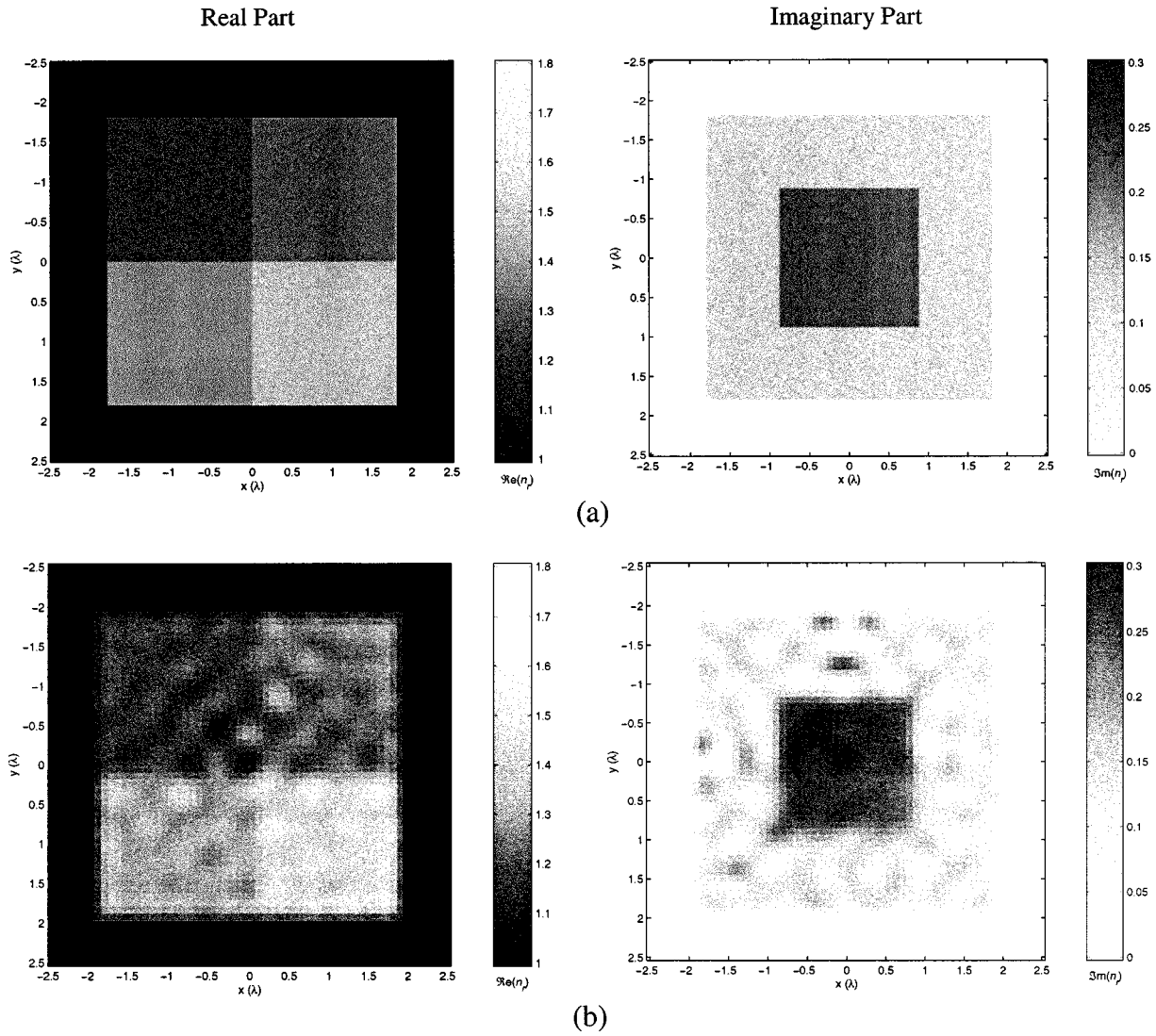

Fig. 6. Exact and reconstructed dielectric profiles. Real part of the refractive index is shown in the left-hand-side column and the imaginary part in the right-hand-side column. (a) Exact profile. (b) Reconstructed profile after 400 iterations.

Although the applicability of the developed algorithm has been demonstrated for microwave tomography, the proposed method is general and can be applied for ultrasonic tomography of biological media since the acoustic-wave propagation is governed by the scalar inhomogeneous Helmholtz equation [35]. An experimental ultrasonic tomography system has been developed and the efficiency of the presented reconstruction method will be further tested using experimental data.

Finally, since the proposed formulation leads to a relatively small number of unknowns, its extension to reconstruct three dimensional (3-D) biological objects may result to a feasible computer implementation. The computational cost associated with the calculation of the integral terms $I(\mathbf{q}, \mathbf{p})$ [see (6)] will increase; however, their calculation can be performed once off-line.

V. Conclusion

A nonperturbative solution for the reconstruction of complex dielectric permittivity based on nonlinear optimization has been presented in this paper. A substantial reduction of the number of optimization variables is achieved for a given problem size, enabling the efficient numerical implementation of the proposed method for electrically large scatterers. The proposed method has been applied for the reconstruction of a biologically relevant dielectric-permittivity profile, as well as for the reconstruction of a square cross-sectional lossy cylinder with a complex structure. The method has no theoretical restriction to weak scattering objects or to objects whose size is small compared to the wavelength.

Appendix

In this appendix, the procedure adopted for the discretization of the spectral-domain integral equations (5) and (7) is described.

By using the Gauss quadrature method of numerical integration and further enforcing (5) at a finite number of wave vectors

$\{\mathbf{q}_m\}$, we obtain a set of linear equations

$$\sum_{l=1}^{M} w(\mathbf{p}_l)C^j(\mathbf{p}_l)\Big[O(\mathbf{q}_m-\mathbf{p}_l)-\lambda^{-2}I(\mathbf{q}_m,\,\mathbf{p}_l)\Big] \cong (2\pi)^2 O\Big(\mathbf{q}_m-\mathbf{k}_{\mathrm{inc}}^j\Big), \qquad m=1,\,\ldots,\,M;\; j=1,\,\ldots,\,J \tag{A1}$$

where $w(\mathbf{p}_l)$ are the weighting coefficients of the quadrature integration, depending solely on the particular selection of the expansion wave vectors $\{\mathbf{p}_l\}$.

If we select the testing wave vectors $\{\mathbf{q}_m\}$ to coincide with the wave vectors used in the quadrature numerical integration, i.e., $\{\mathbf{p}_l\} = \{\mathbf{q}_m\}$, significant computational savings can be achieved by exploiting important symmetry properties of the integrals $I(\mathbf{q}_m,\,\mathbf{p}_l)$ [see (6)], which can be shown by introducing the Gaussian expansion of the object function in (6) and performing some straightforward algebraic manipulations.

The set of equations shown in (A1) can be written in a matrix–vector notation

$$\overline{\mathbf{U}}\mathbf{W}^j = \mathbf{O}^j$$

where the elements of matrix $\overline{\mathbf{U}}$ are given by

$$U_{ml} = O(\mathbf{q}_m-\mathbf{p}_l)-\lambda^{-2}I(\mathbf{q}_m,\,\mathbf{p}_l), \qquad m=1,\,\ldots,\,M;\; l=1,\,\ldots,\,M \tag{A2}$$

and the elements of vectors $\mathbf{W}^j$ and $\mathbf{O}^j$, $j=1,\,\ldots,\,J$ are

$$W_l^j = w(\mathbf{p}_l)C^j(\mathbf{p}_l), \qquad l=1,\,\ldots,\,M$$
$$O_m^j = (2\pi)^2 O(\mathbf{q}_m-\mathbf{k}_{\mathrm{inc}}^j), \qquad m=1,\,\ldots,\,M. \tag{A3}$$

In a similar manner, (7) can be discretized

$$f_{a,\,s}^j = f_a^j(\mathbf{k}_{sc}^s) \cong e^{i(\pi/4)}\frac{\lambda^{-3/2}}{4\pi}\sum_{l=1}^{M} w(\mathbf{p}_l)C^j(\mathbf{p}_l)O(\mathbf{k}_{sc}^s-\mathbf{p}_l), \qquad s=1,\,\ldots,\,S;\; j=1,\,\ldots,\,J \tag{A4}$$

and written in vector notation

$$f_{a,\,s}^j = e^{i(\pi/4)}\frac{\lambda^{-3/2}}{4\pi}(\mathbf{O}^s)^T\,\mathbf{W}^j, \qquad s=1,\,\ldots,\,S;\; j=1,\,\ldots,\,J$$

where the vector $\mathbf{O}^s$ is defined as

$$O_l^s = O\big(\mathbf{k}_{sc}^s-\mathbf{p}_l\big), \qquad l=1,\,\ldots,\,M;\; s=1\ldots S. \tag{A5}$$

REFERENCES

[1] J. R. Shewell and E. Wolf, "Inverse diffraction and a new reciprocity theorem," *J. Opt. Soc. Amer.*, vol. 58, pp. 1596–1603, 1968.

[2] A. J. Devaney, "A filtered backpropagation algorithm for diffraction tomography," *Ultrason. Imaging*, vol. 4, pp. 336–350, 1982.

[3] M. Slaney, A. C. Kak, and L. E. Larsen, "Limitations of imaging with first order diffraction tomography," *IEEE Trans. Microwave Theory Tech.*, vol. MTT-32, pp. 860–873, Aug. 1984.

[4] K. T. Ladas, T. A. Maniatis, and N. K. Uzunoglu, "Inverse scattering using a variational principle," *J. Electromag. Waves Applicat.*, vol. 10, pp. 3–17, 1996.

[5] ——, "On the reconstruction of dielectric objects from scattered field data using the Heitler equation," *Electromag.*, vol. 16, pp. 17–34, 1996.

[6] D. K. Ghodgaonkar, O. P. Gandhi, and M. J. Hagmann, "Estimation of complex permittivities of three-dimensional inhomogeneous biological bodies," *IEEE Trans. Microwave Theory Tech.*, vol. MTT-31, pp. 442–446, June 1983.

[7] S. Caorsi, G. L. Gragnani, and M. Pastorino, "Reconstruction of dielectric permittivity distributions in arbitrary 2-D inhomogeneous biological bodies by a multiview microwave numerical method," *IEEE Trans. Med. Imag.*, vol. 12, pp. 232–239, June 1993.

[8] ——, "Redundant electromagnetic data for microwave imaging of three-dimensional dielectric objects," *IEEE Trans. Antennas Propagat.*, vol. 42, pp. 581–589, May 1994.

[9] W. C. Chew and Y. M. Wang, "Reconstruction of the two-dimensional permittivity using the distorted Born iterative method," *IEEE Trans. Med. Imag.*, vol. 9, pp. 218–255, June 1990.

[10] N. Joachimowicz, C. Pichot, and J. Hugonin, "Inverse scattering: An iterative numerical method for electromagnetic imaging," *IEEE Trans. Antennas Propagat.*, vol. 39, pp. 1742–1752, Dec. 1991.

[11] D. T. Borup, S. A. Johnson, W. W. Kim, and M. J. Berggren, "Nonperturbative diffraction tomography via Gauss–Newton iteration applied to the scattering integral equation," *Ultrason. Imag.*, vol. 14, pp. 69–85, 1992.

[12] A. Franchois and C. Pichot, "Microwave imaging—Complex permittivity reconstruction with a Levenberg–Marquardt method," *IEEE Trans. Antennas Propagat.*, vol. 45, pp. 203–215, Feb. 1997.

[13] N. Joachimowicz, J. J. Mallorqui, J. C. Bolomey, and A. Broquetas, "Convergence and stability assessment of Newton–Kantorovich reconstruction algorithms for microwave tomography," *IEEE Trans. Med. Imag.*, vol. 17, pp. 562–570, Aug. 1998.

[14] A. E. Souvorov, A. E. Bulyshev, S. Y. Semenov, R. H. Svenson, A. G. Nazarov, Y. E. Sizov, and G. P. Tatsis, "Microwave tomography: A two-dimensional Newton iterative scheme," *IEEE Trans. Microwave Theory Tech.*, vol. 46, pp. 1564–1659, Nov. 1998.

[15] A. Roger, "A Newton–Kantorovich algorithm applied to an electromagnetic inverse problem," *IEEE Trans. Antennas Propagat.*, vol. AP-29, pp. 232–238, Mar. 1981.

[16] H. T. Lin and Y. W. Kiang, "Microwave imaging for a dielectric cylinder," *IEEE Trans. Microwave Theory Tech.*, vol. 42, pp. 1572–1579, Aug. 1994.

[17] R. Kleinman and P. M. van den Berg, "An extended range-modified gradient technique for profile inversion," *Radio Sci.*, vol. 29, pp. 877–884, 1993.

[18] B. J. Kooij and P. M. van den Berg, "Nonlinear inversion in TE scattering," *IEEE Trans. Microwave Theory Tech.*, vol. 46, pp. 1704–1712, Nov. 1998.

[19] T. M. Habashy, M. L. Oristaglio, and A. De Hoop, "Simultaneous nonlinear reconstruction of two-dimensional permittivity and conductivity," *Radio Sci.*, vol. 29, pp. 1101–1118, 1994.

[20] P. van den Berg and R. E. Kleinman, "A contrast source inversion method," *Inverse Problems*, vol. 13, pp. 1607–1620, 1997.

[21] S. Caorsi, G. L. Gragnani, M. Pastorino, and M. Rebagliati, "A model-driven approach to microwave diagnostics in biomedical applications," *IEEE Trans. Microwave Theory Tech.*, vol. 44, pp. 1910–1920, Oct. 1996.

[22] I. T. Rekanos, T. V. Yioultsis, and T. D. Tsiboukis, "Inverse scattering using the finite-element method and a nonlinear optimization technique," *IEEE Trans. Microwave Theory Tech.*, vol. 47, pp. 336–344, Mar. 1999.

[23] K. D. Paulsen, P. M. Meaney, M. J. Moskowitz, and J. M. Sullivan Jr., "A dual mesh scheme for finite element based reconstruction algorithms," *IEEE Trans. Med. Imag.*, vol. 14, pp. 504–514, Sept. 1995.

[24] L. E. Larsen and J. H. Jacobi, "Microwave scattering parameter imagery of an isolated canine kidney," *Med. Phys.*, vol. 6, pp. 394–403, 1979.

[25] A. Franchois, A. Joisel, C. Pichot, and J. C. Bolomey, "Quantitative microwave imaging with a 2.45-GHz planar microwave camera," *IEEE Trans. Medical Imaging*, vol. 17, pp. 550–561, Aug. 1998.

[26] A. Broquetas, J. Romeu, J. M. Rius, A. R. Elias-Fuste, A. Cardama, and L. Jofre, "Cylindrical geometry: A further step in active microwave tomography," *IEEE Trans. Microwave Theory Tech.*, vol. 39, pp. 836–844, May 1991.

[27] S. Y. Semenov, R. H. Svenson, A. E. Boulyshev, A. E. Souvorov, V. Y. Borisov, Y. Sizov, A. N. Starostin, K. R. Dezern, G. P. Tatsis, and V. Y. Baranov, "Microwave tomography: Two-dimensional system for biological imaging," *IEEE Trans. Biomed Eng.*, vol. 43, pp. 869–877, Sept. 1996.

[28] S. Y. Semenov, A. E. Boulyshev, A. E. Souvorov, R. H. Svenson, Y. E. Sizov, V. Y. Borisov, V. G. Posukh, I. M. Kozlov, A. G. Nazarov, and G. P. Tatsis, "Microwave tomography: Theoretical and experimental investigation of the iteration reconstruction algorithm," *IEEE Trans. Microwave Theory Tech.*, vol. 46, pp. 133–141, Jan. 1998.

[29] P. M. Meaney, K. D. Paulsen, and J. T. Chang, "Near-field microwave imaging of biologically based materials using a monopole transceiver system," *IEEE Trans. Microwave Theory Tech.*, vol. 46, pp. 31–45, Jan. 1998.

[30] A. J. Devaney and G. Beylkin, "Diffraction tomography using arbitrary transmitter and receiver surfaces," *Ultrason. Imag.*, vol. 6, pp. 181–193, 1984.

[31] H. P. Schwan and K. R. Foster, "RF field interactions with biological systems: Electrical properties and biophysical mechanism," *Proc. IEEE*, vol. 68, pp. 104–113, Jan. 1980.

[32] C. Gabriel, S. Gabriel, and E. Corthout, "The dielectric properties of biological tissues," *Med. Phys.*, vol. 41, pp. 2231–2293, 1996.

[33] D. Colton and R. Kress, *Inverse Acoustic and Electromagnetic Scattering Theory*. Berlin, Germany: Springer-Verlag, 1998.

[34] J. H. Richmond, "Scattering by a dielectric cylinder of arbitrary cross-section shape," *IEEE Trans. Antennas Propagat.*, vol. AP-13, pp. 334–341, May 1965.

[35] B. S. Robinson and J. F. Greenleaf, "The scattering of ultrasound by cylinders: Implications for diffraction tomography," *J. Acoust. Soc. Amer.*, vol. 80, pp. 40–49, 1986.

Theofanis A. Maniatis (M'00) was born in Athens, Greece, in 1967. He received the Diploma degree in electrical engineering from the National Technical University of Athens, Athens, Greece in 1990, the M.A.Sc. degree from the University of Toronto, Toronto, ON, Canada, in 1993, and the Ph.D. degree from the National Technical University of Athens, Athens, Greece, in 1998.

Since 1999, he has been a Researcher at the Institute of Communication and Computer Systems, National Technical University of Athens. His research interests include inverse scattering, computational electromagnetics, and medical imaging.

Dr. Maniatis is a member of the Technical Chamber of Greece and the Hellenic Society of Biomedical Engineering.

Konstatina S. Nikita (M'96–SM'00) received the Diploma degree in electrical engineering and the Ph.D. degree from the National Technical University of Athens, Athens, Greece, in 1986 and 1990, respectively, and the M.D. degree from the Medical School, University of Athens, Athens, Greece, in 1993.

Since 1990, she has been a Researcher at the Institute of Communication and Computer Systems, National Technical University of Athens. In 1996, she joined the Department of Electrical and Computer Engineering, National Technical University of Athens, where she is currently an Assistant Professor. Her current research interests include applications of electromagnetic waves in medicine, electromagnetic scattering, diffraction tomography, medical imaging and image processing, and nonlinear optimization algorithms and applications. She has been the Technical Manager of a number of European and National Research and Development projects in the field of biomedical engineering.

Dr. Nikita is a member of the Technical Chamber of Greece, the Athens Medical Association, and the Hellenic Society of Biomedical Engineering.

Nikolaos K. Uzunoglu (M'82–SM'97) was born in Constantinopole, in 1951. He received the B.Sc. degree in electronics from the Technical University of Istanbul, Istanbul, Turkey, in 1973, the M.Sc. and Ph.D. degrees from the University of Essex, Essex, U.K., in 1974 and 1976, respectively, and the D.Sc. degree from the National Technical University of Athens, Athens, Greece, in 1981.

From 1977 to 1984, he was a Research Scientist in the Office of Research and Technology of the Hellenic Navy. In 1984, he became an Associate Professor at the National Technical University of Athens, Department of Electrical Engineering and, in 1987, he became a Professor. In 1986, he was elected Vice-Chairman of the Department of Electrical Engineering, National Technical University of Athens and, in 1988, he became Chairman of the same department. He was reelected as Chairman in 1990 and 1992 twice. In 1991, he became Director of the Institute of Communication and Computer Systems, an independent research establishment associated with the National Technical University of Athens, and served in this position until 1999. He has authored or co–authored over 120 papers in refereed international journals, and has authored three books in Greek on microwaves, fiber-optic telecommunications, and radar systems. His research interests include electromagnetic scattering, propagation of electromagnetic waves, fiber-optic telecommunications, and high-speed circuits operating at gigabit/second rates. Since 1988 he has been the national representative of Greece to the COST, Technical Telecommunications Committee, and has actively participating in several COST telecommunications projects. Further, he has been Project Manger of several RACE, ESPRIT, ACTS and National Research and Development Projects in the fields of telecommunications and biomedical engineering applications.

Dr. Uzunoglu was the recipient of the 1981 International G. Marconi Award in Telecommunications. In 1994, he was elected as an Honorary Professor of the State Engineering University of Armenia. He was awarded the honorary Ph.D. diploma from the Universities of Bucharest, Cluj-Napoca, and Orade. In 1998, he was elected a Foreign Member of the National Academy of Sciences of Armenia.